



International Commission on Illumination
Commission Internationale de l'Eclairage
Internationale Beleuchtungskommission

THE EFFECT OF RADIATION PATTERNS ON VEHICULAR VISIBLE LIGHT COMMUNICATION

Dotreppe, G.M., et al.

DOI 10.25039/x051.2025/6q626j

This article is also published as part of:

Proceedings of the CIE 2025 Midterm Meeting Vienna, Austria, July 4-11, 2025:
Scientific Conference (July 7-9, 2025)

DOI 10.25039/x051.2025

in

Proceedings of the CIE (International Commission on Illumination)

ISSN no. 3061-015X (print), 3061-0168 (online)

The paper has undergone double-blind peer review and its final version has been presented at the CIE 2025 Midterm Meeting, Vienna, Austria, July 4–11, 2025.

© CIE 2025

All rights reserved. This work is licensed under the Creative Commons Attribution-NonCommercial 4.0 International License (<https://creativecommons.org/licenses/by-nc/4.0/>). Any mention of organizations or products does not imply endorsement by the CIE.

CIE Central Bureau
Babenbergerstrasse 9/9A
A-1010 Vienna, Austria
Tel.: +43 1 714 31 87
e-mail: ciecb@cie.co.at — www.cie.co.at

THE EFFECT OF RADIATION PATTERNS ON VEHICULAR VISIBLE LIGHT COMMUNICATION

Dotreppe, G.M.¹, Coosemans, J.M.¹, Van den Bossche, P.¹ Jacobs, V.A.¹

¹ Vrije Universiteit Brussel — Merlin at MOBI research group, Brussels, Belgium;

guillaume.mario.dotreppe@vub.be

Abstract

Vehicular Visible Light Communication (V-VLC) offers a compelling alternative communication technology for Intelligent Transportation Systems, leveraging its license-free spectrum, wide bandwidth, energy efficiency, and existing transmitters. Accurate optical channel modelling is essential for evaluating V-VLC feasibility and performance in vehicular environments. For this, accurate transmitter representations are required. Low beam headlights and daytime running lights are primary candidates for VLC transmitters, yet simplified light source models often lack photometric realism compared to actual vehicle headlights. A comparison of a Lambertian and a measured low-beam emission patterns reveals that Lambertian models underestimate communication range while overestimating mobility. A narrow beam better reflects the low beam irradiance but requires careful design considerations for an optimal representation. This study examines the differences between the source models commonly used and suggests alternative modelling approaches depending on the communication range.

Keywords: e.g. Photometry, Vehicle Lighting, VLC, Channel Modelling

1 Introduction

Despite a downward trend in road-related fatalities, traffic incidents in 2018 were the main cause of death among young people/adults and rank as the 8th leading cause of mortality worldwide, as reported by the *World Health Organization: Global Status Report On Road Safety 2018* (WHO, 2018, Cailean and Dimian, 2017). Today, the World Health Organization reports that traffic incidents are still the leading cause of death among young people and adults between 5 and 29 years old (WHO, 2023). Therefore, bolstering road safety remains paramount. Advanced Driver Assistance Systems, Intelligent Transportation Systems (ITS), and autonomous vehicles (AV) within vehicle fleets offers a significant path forward (Cailean and Dimian, 2017). The widespread adoption of these technologies relies on advancements in vehicular wireless communication.

Within the realm of wireless communication technologies, Visible Light Communication (VLC) offers an interesting alternative to traditional radio frequency (RF) based communication systems. Unlike the licensed RF spectrum, VLC exploits an unlicensed portion of the electromagnetic spectrum for data transmission (Memedi and Dressler, 2020). By modulating light from existing sources such as streetlights or headlights, bi-directional links with data rates 100 times larger than those offered by Wi-Fi are achievable (Van Mierlo et al., 2021, Shaaban et al., 2021). For vehicular applications, this technology is referred to as vehicular visible light communication (V-VLC).

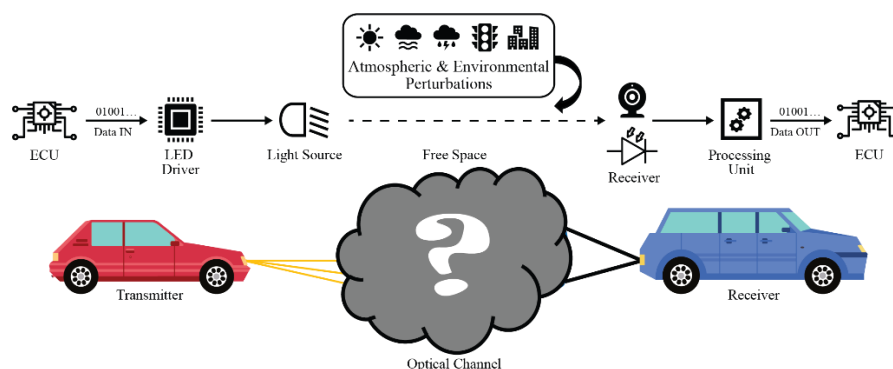


Figure 1 – Schematic overview of the V-VLC working principle. The cloud in between transmitting and receiving vehicle represents the optical channel model requiring more attention.

Figure 1 provides a schematic overview of the V-VLC topology, incorporating considerations of link geometry and atmospheric influences that impact communication quality between transmitter and receiver, as modelled through the optical channel. The feasibility and performance assessment of a V-VLC system begins with analysing the geometric characteristics of the optical channel. Paramount herein is the light source representation/modelling. Recent research mainly considers simplified transmitter characteristics: a radiating point source with a generalised Lambertian luminous intensity distribution (Ndjiongue and Ferreira, 2018, Memedi and Dressler, 2020). A generalised Lambertian distribution refers to a Luminous Intensity Distribution (LID) with a power cosine distribution:

$$I(A, \alpha) = I_0 \cos^n(\alpha) \tag{1}$$

With I_0 the peak intensity along the optical axis, α the emission angle, and A the considered emission plane in an $A - \alpha$ references coordinate system (CIE 121, 1996). n determines the Full Width at Half Maximum (FWHM) of the light source. The higher the value of n , the narrower the beam. These rotational symmetric LIDs, however, do not represent vehicle headlights accurately which are bound to stringent regulations in terms of beam shape. Therefore, in this study the influence of having beam shapes different from a generalised Lambertian is investigated considering the spatial optical power distribution of the luminaires. Using a ray file obtained through a near field imaging luminance measurement, ray tracing simulations are performed capturing the optical power emitted by a low beam for a range of relevant detector positions. The results are compared to the point source representation of the low beam, a Lambertian, and narrow beam as these are most used for channel modelling purposes.

2 Materials and methods

This section briefly describes the current channel model practices, highlighting common trends and shortcomings. The according regulations relevant to vehicle lighting systems for V-VLC are discussed. Finally, the measurement procedure required for improved channel models is presented.

2.1 Channel models

VLC can be modelled as a Linear Time Invariant (LTI) system (Yahia et al., 2018, Hasan et al., 2022):

$$P_R(t) = P_T(t) * h(t) + N(t) \tag{2}$$

with $P_R(t)$ [W] the received optical power, $P_T(t)$ [W] the transmitted optical power, $h(t)$ the channel impulse response (CIR) and $N(t)$ the detector noise. The CIR consists of both the Line-of-Sight (LOS) and Non-Line-of-Sight (NLOS) components. In this paper, only the LOS component is considered to assess the geometrical attenuations of the optical channel using optical path losses (PLs), i.e. the decay in received signal strength during its propagation through free space. The PL determines the required emission power of the source and the sensitivity of the receiver, resulting in one of the most critical characteristics of a VLC system (Alsalami et al., 2021). The geometrical losses are characterised by the link geometry, represented by the channel Direct Current (DC) gain $H(0)$ as the time averaged CIR (Ghassemlooy et al., 2019, Yahia et al., 2021). It relates the average optical power received by the detector to the total emitted power by the light source (Memedi and Dressler, 2020, Yahia et al., 2021, Shaaban and Faruque, 2020):

$$H(0) = \int_0^\infty h(t)dt = \frac{P_R}{P_T} \tag{3}$$

The VLC channel gain in decibels represents the PLs:

$$PL = -10\log_{10}H(0) \tag{5}$$

The DC channel gain is mostly modelled using either an analytical or empirical approach. **Analytical models** allow to analyse the optical channel considering various influencing factors independently (e.g. weather conditions, inter-vehicular distance, road conditions, etc.). While powerful for preliminary studies, these models lack versatility because they require a functional representation of the light source distribution. Vehicle lights are mainly represented as a symmetrical Lambertian or Gaussian distribution. The analytical channel DC gain derived using

Eq. (1) for the LID define the geometrical losses due to a generalised Lambertian light distribution:

$$H(0) = \begin{cases} \frac{n+1}{2\pi} \cos^n(\alpha_s) \frac{\cos(\alpha_r)}{d^2} A, & 0 \leq \alpha_r \leq \alpha_{r,c} \\ 0, & \alpha_r > \alpha_{r,c} \end{cases} \quad (6)$$

The Field-of-View (FOV) of the detector is given by $\alpha_{r,c}$. Note that this approach is only valid for a point source radiator.

Because the generalised Lambertian LID fails to accurately represent a low beam, and deriving a functional relationship representing the latter proves difficult, alternative modelling approaches have been explored. **Empirical models**, such as those by Tseng et al. (2015), present the most realistic channel to date. These involve either real-world testing of V-VLC system performance under specific conditions or the measurement of a source's LID for subsequent path loss computation. However, the former present uncertainties due to external factors influencing the measurements, often difficult to decouple from the quantity of interest. Furthermore, the measurements only reflect the performance for the tested scenario, rendering generalisation of the results complicated. LID measurements themselves are frequently conducted without adherence to standard photometric procedures, such as minimum test distances or inclusion of relevant emission planes. Moreover, some studies incorrectly apply high beam headlamp data to model LBs or taillights.

Indirect representations of the channel are derived through **Monte Carlo simulations** and **Machine Learning** techniques. Monte Carlo simulations use probability density functions to statistically model time-dependent scenarios, making them suitable for capturing the dynamic vehicular environment, including mobility, weather conditions, and NLOS characteristics. Machine learning, though still developing, holds promise for modelling complex multi-factor environments, particularly in end-to-end channel optimisation. However, such models require large volumes of high-quality training data, and the lack of transparency in experimental setups often hinders validation and reproducibility.

Ray tracing simulations bridge the gap between the two approaches as the ray files stem from either an analytical or empirical origin. While versatile and accurate, the long computation times and stochastic source representation still present some challenges. Furthermore, in the field of V-VLC channel modelling, the full capabilities of ray tracing simulations, allowing to capture the extended nature of the vehicle headlights, are still lacking.

Regardless of the method employed, most models only consider the horizontal and vertical planes intersecting the photometric centre of the headlamp. This approach overlooks the structured distribution of regulated LBs, particularly the sharp cut-off line. In this study, various source models are evaluated using both analytical calculations and ray tracing-based path loss estimations.

2.2 Headlight regulations

Commonly used light sources under typical driving conditions, namely daytime running lights (DRLs) and low beams, present the best candidate for a V-VLC transmitter. These sources are subject to specific requirements regarding mounting positions, orientations, beam patterns, and maximum light output which need to be considered for an improved geometric channel representation. UN/ECE R48 (2018) is an overarching standard governing the installation of all lighting devices on a vehicle. This covers the positioning and number of light sources amongst others. Specific regulations on the lighting quality in terms of light intensity, beam pattern, colour temperature, alignment, aiming and compliance testing are provided in UN/ECE R87 (2009) and R112 (2013) for DRLs and LBs respectively. Regulation No. 128 (2018) covers the approval of LED light sources for a vehicular environment regarding colorimetric and photometric properties. Testing standards are defined as well to ensure consistency in the performance and safety of LED lighting. Finally, UN/ECE R149 (2021) consolidates and advances regulations for headlamp systems, especially with the advent of intelligent lighting technologies. It supersedes older regulations to harmonise and modernise requirements to current lighting systems. The standardised, minimal, testing distance for the intensity distribution of low beams is 25 m. Measuring the quality of the cut-off line is permitted at 10 m provided the detector aperture is modified accordingly.

2.3 Headlight Measurements

Given the limited availability of headlight beam patterns, measurements of a Hella R80 low beam headlight intended for right hand driving were conducted. Ray files have been generated from near-field (NF) measurements using a TechnoTeam RIGO 801-L Imaging Luminance Measurement Device (ILMD) based goniophotometer. It is equipped with an LMK 98-4 DMX4-285 luminance camera and a Czibula & Grundmann Standard-photometer head. A calibrated Keithley 2425 100W SourceMeter has been used to feed a controlled current to the light sources. The measured ray files are imported in Lambda Research’s TracePro ray tracer for further manipulation. To preserve realistic simulation times, 100 million rays per light source are used, randomly generated from the 1 billion rays measured. Note, that ray tracing simulations operate on a stochastic basis, with a decreasing signal-to-noise ratio at greater distances due to a reduced ray density. Hence, this limits the practical simulation distance.

2.4 Geometrical Configuration

The optical power is recorded at positions representing typical inter-vehicular distances on a three-lane roadway. The distances vary depending on the environment, such as urban, highway, or rural settings, and prevailing road conditions. To account for a broad spectrum of scenarios, distances ranging from 2 m to 50 m are considered (Al-Sallami et al., 2024, Shaaban and Faruque, 2020). The maximum reported lane width of 3.75 m is adopted to account for the widest possible lateral displacements (Liu et al., 2023, ERSO, 2018, Teodorović and Janić,2017).

The transmitter and receiver surfaces are assumed to remain perfectly parallel for all relative positions, as shown in Figure 2 graphically representing the considered geometry. Two scenarios are considered: a single headlight configuration and a dual headlight configuration. In line with UN/ECE Regulation R48 (2018), the dual-headlight configuration assumes a mounting height of 700 mm and a centre-to-centre spacing of 1400 mm between two low beam sources. In the single-source scenario, a single LB is placed at the centre of the middle lane, allowing to evaluate the coverage area of an individual transmitter. The geometric centre of the transmitter is aligned with the centre of the middle lane.

The receiving surface is modelled as a circular detector with a 50 mm diameter, consistent with the photometer used in the photometric tunnel. For each considered distance, detectors are arranged in a 101-by-25 grid, spanning the full roadway width in the horizontal (y) direction. Vertically (z -direction), the grid extends from the road surface (0 m) up to a height of 3 m, thereby capturing various potential detector positions on vehicles.

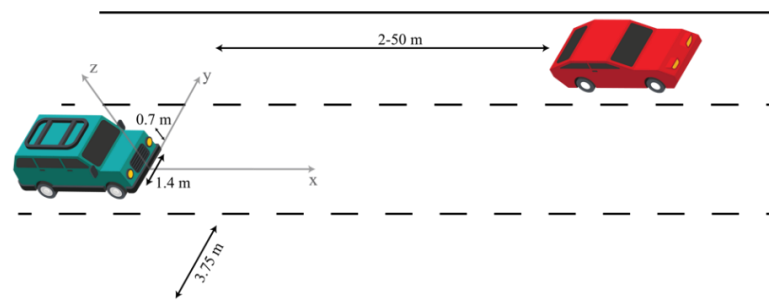


Figure 2: Geometrical configuration considered between a transmitting (green) and a receiving vehicle (ref) on a three-lane road. The dual low beam configuration is depicted.

2.5 Source modelling

Representing the transmitters as radiating point sources is computationally the most efficient. However, this representation is only valid from a certain distance on, referred to as the Limiting Photometric Distance (LPD). For distances shorter than the LPD, the point source assumption fails, and the extended nature of the radiating surface is to be considered (Dotreppe et al., 2023).

For the vehicle low beam, the received optical power at different detector locations is obtained through ray tracing simulations, accurately representing its extended nature. The optical power is extracted from the number of rays intersecting with the detector. Each ray carries an optical power equivalent to a fraction of the total luminous flux. When two low beams are considered, each source is assumed identical.

The path losses obtained through the ratio of received to total optical flux as estimated using ray tracing simulations are compared with the ones computed from a point source representation of the low beam. Furthermore, a comparison is carried out with a Lambertian ($n = 0$; $FWHM = 60^\circ$) and narrow beam ($n = 180$; $FWHM \approx 10^\circ$) LID following Eq. (1). In this case, the channel DC gain is directly extracted from Eq. (6). The narrow beam FWHM is equivalent to the largest beam extend of the low beam, in the horizontal direction.

Table 1 summarises the various simulation parameters employed. The peak intensity values are extracted from the luminous flux of the measured low beam applied to all LIDs. The peak intensity of the Lambertian indicates a noticeably less concentrated distribution compared to the LB. The narrow beam shows a closer match, yet still diverges from the real low beam.

Table 1: Summary of the source LID characteristics

	Low Beam Near-Field	Lambertian FWHM = 60°	Narrow Beam FWHM $\approx 10^\circ$
Luminous flux [lm]	700.1	700.1	700.1
Luminous surface diameter [mm]	90	N/A	N/A
Peak intensity [cd]	31329	222.8	20390.1
Peak intensity plane (A) [$^\circ$]	1	0	0
Peak intensity direction (α) [$^\circ$]	-2.4	0	0
Number of rays [-]	99904156	N/A	N/A
Sample points	N/A	10000	10000

3 Results and discussion

The different modelling approaches for a V-VLC system are analysed in this section, first comparing the LIDs of the different sources, and then the associated path losses. The ray tracing simulations considering the low beam extended nature are taken as reference.

3.1 LID Comparison

A comparison of the different considered LIDs is presented in Figure 3 as the projected relative illuminance on a horizontal plane at the standardised measurement distance of 25 m (UN/ECE, 2021). A clear distinction between the generalised Lambertian profiles and the measured low beams is observed. The latter displays a strong cut-off line and a wider horizontal than vertical distribution. This is in accordance with its purpose to be illuminate the road surface, avoiding glare for the oncoming traffic (in this case, at the left-hand side).

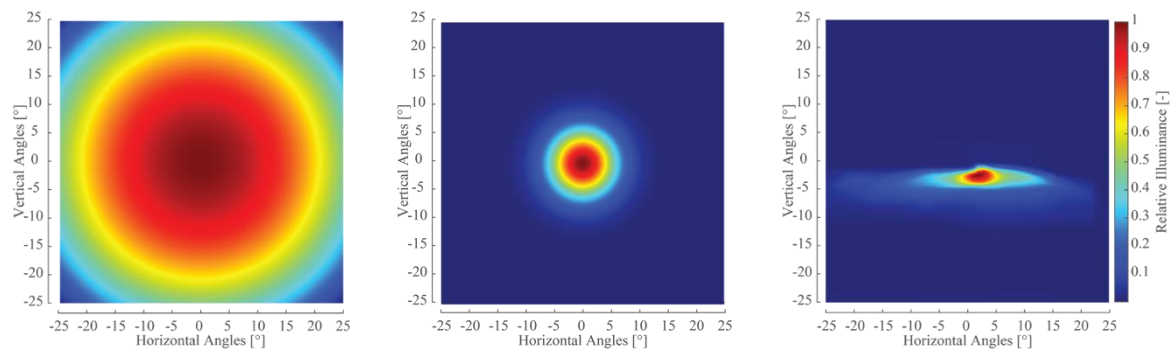


Figure 3: Comparison between the projected horizontal relative illuminance at 25m for a Lambertian source ($n=0$) (left), narrow beam ($n = 180$) (middle) and a LB (right). All sources have identical physical dimensions.

Figure 4 shows the intensity profiles for four A-planes, normalised to the peak value of the respective intensity distributions to alleviate discrepancies due to the measurement setup. Each A-plane represents a vertical slice of the LID shown in Figure 3 (see CIE 121-1996). The profiles are presented as if an observer was looking at a car from the side. A downwards oriented intensity for the low beams is observed. Similar distributions shapes are observed for all A-planes, however increasing in amplitude until a maximum is reached at $A = 1^\circ$. The intensity profiles then decrease, until negligible values are achieved for $A > 25^\circ$.

The Lambertian distribution shows a rotational symmetry along the α -angles with a more constant profile. Only small variations in the considered range are observed owing to its

spherical intensity distribution following a cosine. For example, the largest intensity value for $A = 25^\circ$ is still $> 90\%$ of the peak intensity, as $\cos(25^\circ) = 0.9063$. The narrow beam also presents rotational symmetry for all A -planes yet decreases strongly in amplitude as the A -plane diverges from $A = 0^\circ$. For planes larger than twice the FWHM angle of the source, the intensity values become negligible.

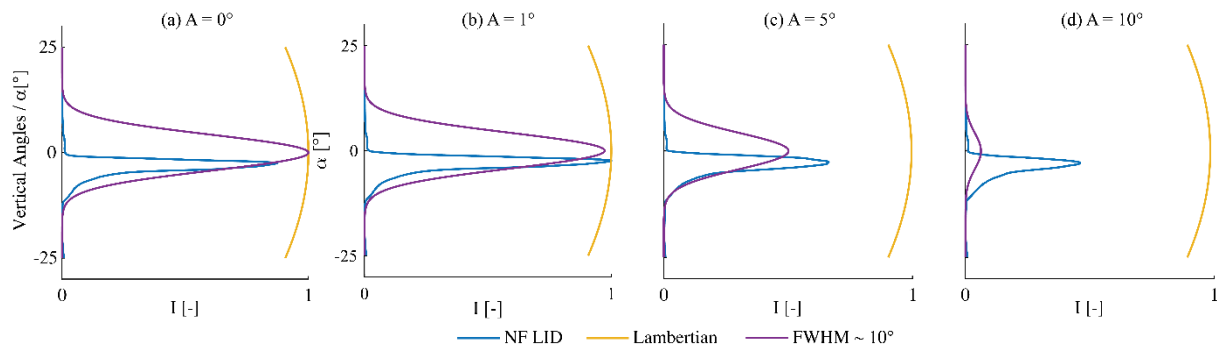


Figure 4: Comparison between the normalised NF, FF, Lambertian and narrow beam LID profiles for 4 different A -planes. These represent vertical slices in the profiles shown in Figure 3.

Finally, Figure 5 shows the LID profile in a horizontal plane, at an angle $\alpha = -2.4^\circ$ compared to the horizon. This represents a horizontal slice of Figure 3 at a vertical angle of -2.4° , the α -angle for peak intensity of the NF measured low beam. The low beam exhibits a higher intensity value for the right-hand direction, opposite to the oncoming traffic. The other LIDs show rotational symmetry along the vertical plane ($A = 0^\circ$). The Lambertian shows a limited variation of its intensity. The narrow beam does not reach its peak value, as this is located along the optical axis at $A = 0^\circ$ and $\alpha = 0^\circ$. Neither simplified models accurately represent the asymmetrical LB profile.

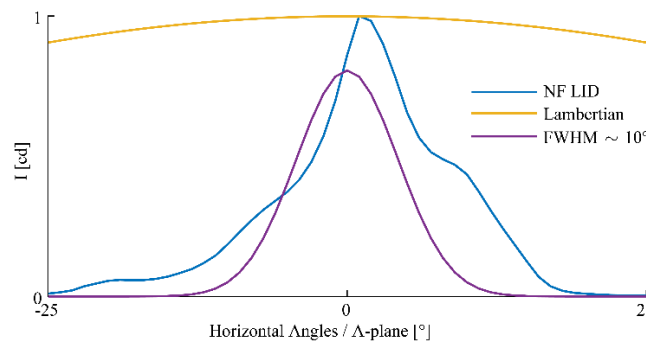


Figure 5: Comparison between the normalised NF, FF, Lambertian and narrow beam LID profiles for a horizontal plane located below the horizon. This represents a horizontal slice in the profiles shown in Figure 3.

This comparison indicates that, when normalised to identical peak intensities, the Lambertian distribution consistently overestimates the channel capacity across all emission planes. The narrow beam likewise overestimates the channel capacity for angles aligned with or above the photometric axis ($\alpha \geq 0^\circ$), but underestimates it in downward directions, where the real low beam contributes most significantly to road illumination. Although the low beam maintains a relatively stable angular distribution across planes, its absolute intensity varies notably, peaking at $A = 2^\circ$ and $\alpha = -2.4^\circ$, before decreasing rapidly. Importantly, achieving comparable peak intensities using Lambertian or power-cosine LIDs would require substantially higher luminous flux, which would result in excessive glare for oncoming drivers, rendering such configurations impractical and non-compliant with vehicular lighting regulations.

3.2 V-VLC Path Loss Comparison

3.2.1 Extended VS Point Source Representation

Figure 6 illustrates the evolution of the low beam intensity projected onto a vertical surface at increasing distances. A downward-facing, diverging beam profile is clearly observed. At short ranges (less than 5 m), the optical power is concentrated within a narrow area, aligned with the mounting height of the source. As the distance increases, the beam diverges, illuminating a broader area while reducing the flux per unit area (or per pixel). Consequently, although the coverage area expands with distance, the transmission speed is expected to decrease due to

a reduced signal-to-noise ratio. Moreover, as the beam travels further, an increasing portion of the emitted light reaches the road surface, introducing non-line-of-sight components. Depending on the receiver configuration, these components may need to be considered, as they can account for a significant portion of the total emitted flux.

Precisely defining the LPD by comparing ray tracing results becomes challenging due to the increasing statistical error at longer evaluation distances. However, an approximate LPD can be inferred by computing the root mean square percentage error (RMSPE) between ray tracing results and point source approximations. When the RMSPE reaches below a certain threshold value, the difference between using the point source approximation and the extended source representation becomes negligible within the threshold boundary. The RMSPE demonstrates a decreasing trend with distance, reaching a minimum at approximately 17 m, after which it begins to rise again. This suggests that a minimum distance of 17 m is required for a single LB source to be accurately represented as a point source. The increase in RMSPE is due to the increasing statistical error from a certain distance on.

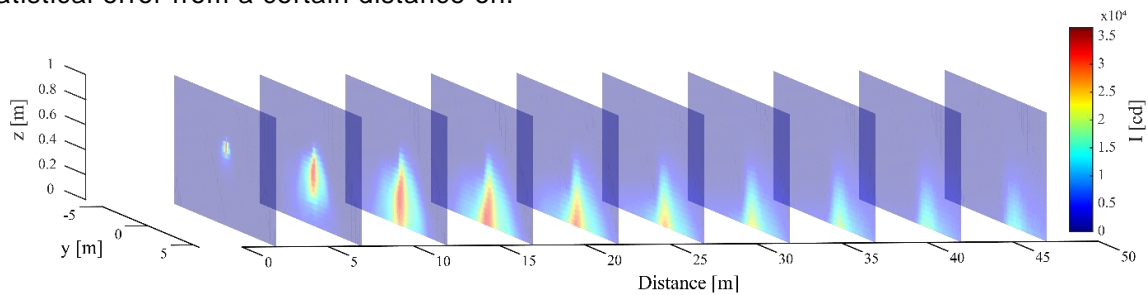


Figure 6: Projected intensity distribution of the low beam on vertical planes at various distances.

Despite the above threshold distance, because the point source approximation is often applied for arbitrary distances a comparison between the different LB modelling approaches is presented for a distance of 8 m, corresponding to a typical inter-vehicle distance while driving (Shaaban and Faruque, 2020). Figure 7 presents the comparison between the models using the path loss difference L_P [dB], computed as:

$$L_P = PL_{Test} - PL_{Ref} = 10 \log_{10} H(0)_{Test} - 10 \log_{10} H(0)_{Ref} = 10 \log_{10} \left(\frac{P_{R,Test}}{P_{R,Ref}} \right) \quad (7)$$

Here, the received optical power of the low beam $P_{R,Ref}$, as obtained via ray tracing simulations, serves as the reference. The metric L_P thus quantifies the ratio of received powers.

Using the LID to model the low beam instead of ray tracing simulations yields only minor deviations, primarily near the cut-off line and in regions with large optical gradients. Figure 7(a) reveals a peak overestimation of the former approach near the cut-off line at approximately $z \simeq 0.5$ m and $y \simeq 0$ m, and an underestimation near the LB profile edges, with the most pronounced underestimation occurring around $z \leq 0.5$ m and $y \simeq \pm 4$ m. Variations observed at the edges of the measurement screen can largely be attributed to the stochastic nature of the ray tracing simulations.

Figure 7(d) shows the same comparison for a dual-source configuration, with the colour scale matched to that in 7(a) for direct comparison. Similar trends are observed, with two overestimation peaks corresponding to the cut-off lines of the individual sources. At the profile edges, an underestimation is again noted, though now at wider positions due to the lateral displacement of each source relative to the screen's centre. This spatial offset increases the intensity at the screen's periphery, thereby reducing the variation in path loss.

Overall, a decent agreement between the models is observed. The deviations can be mainly attributed to the discrete and probabilistic nature of the ray tracing model. In particular, larger discrepancies appear at the lateral edges of the screen, where ray density is lower and variability is higher. These effects may be compounded by stray light captured during source measurements, but are primarily a result of the finite number of rays used to represent the emitted flux in each direction. In contrast, the LID-based model produces a smoother intensity profile, due to its continuous nature and the use of linear interpolation to estimate values for arbitrary directions.

3.2.2 Extended Low Beam VS Lambertian Point Source

Comparing the low beam with the Lambertian, a large discrepancy can be observed, as shown in Figure 7(b). The Lambertian resulted in a strong underestimation of the optical power received in the lower region, within a vertical region of ± 4 m, where the low beam provides most of its illumination. At other locations, the Lambertian overestimates the optical power due to its wider beam divergence. At the roadway sides, the Lambertian results in an optical power up to 100 times larger than the low beam. The dual source profile shows a similar behaviour, but the vertical region of underestimation is widened to $y = \pm 5$ m, as illustrated in Figure 7(e). This is because the optical power is doubled, and the spatial distribution slightly widened due to the source's physical separation

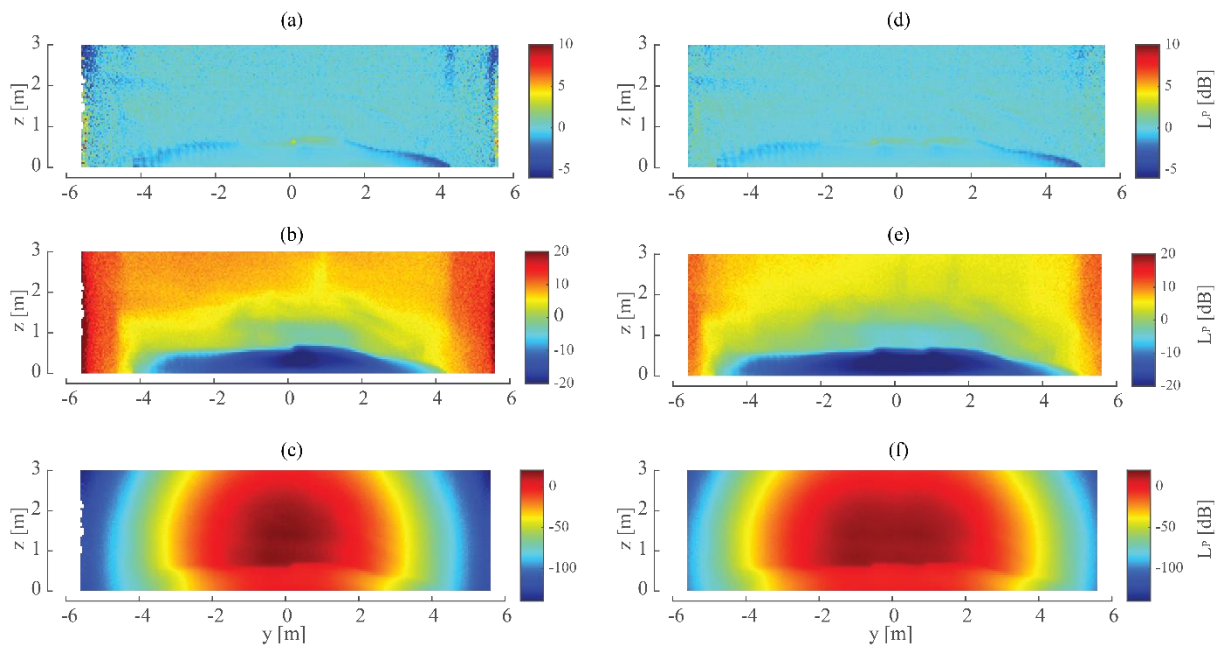


Figure 7: PL difference L_p between the ray tracing simulated low beam and the point source representation of: the low beam, Lambertian and narrow beam model (top to bottom). The left figures are for a single source, the right figures for a dual source system.

3.2.3 Extended Low Beam VS Narrow Beam Point Source

Figure 7(c) shows that the narrow beam source exhibits an overestimation of the received optical power in the vicinity of its peak intensity. However, this overestimation is confined to a single lane, with a sharp decline in optical power observed in adjacent lanes due to the beam's limited spread. In the region most strongly illuminated by the low beam, the narrow beam continues to underestimate the received power. This behaviour is illustrated in Figure 8 using a logical comparison. Positive L_p values, indicating an overestimation of the narrow beam relative to the low beam, are represented as logical 1 and shown in red, while underestimations are denoted as logical 0 and appear in blue. The axially symmetric nature of the beam profile is clear, with underestimation occurring primarily in the region of high illumination produced by the low beam (lower central area), as well as in peripheral regions where neither source contributes significantly to illumination (upper corners).

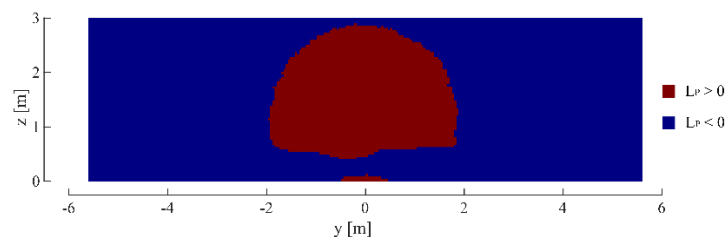


Figure 8: Logic comparison between the PLs of the single narrow beam and low beam source. When the NB overestimates the path losses of the low beam, an $L_p > 0$ is computed, and a logic 1 is obtained, shown in red. Inversely, a logic 0 is obtained, shown in blue.

The dual source model results in the same observations as for the Lambertian, with a wider underestimation region due to the spatial separation of the sources, as depicted in Figure 7(f). Despite these discrepancies, the narrow beam provides a more faithful representation of the low beam than the Lambertian source, particularly in critical regions, where overall L_p values are lower. Dual-source systems do not exhibit any substantial deviations from these observations.

3.3 Discussion

From the above, it can be inferred that the concentrated emission pattern of the LB significantly limits the mobility of a V-VLC system when compared to a Lambertian source, which provides higher illuminance levels over a broader angular range. However, achieving the minimum intensity values specified by the UN/ECE R112 standards using a Lambertian distribution necessitates a substantial increase in luminous flux, which would result in intolerable glare for other road users. Consequently, the Lambertian source is not a realistic representation of vehicle headlights in practical scenarios and is therefore unsuitable for accurately modelling the performance of a V-VLC system.

In contrast, the narrow beam source more closely replicates the distribution of vehicle headlights within a region around the low beam cut-off lines. However, as the angle deviates from this region, the NB strongly overestimates the received optical power around its optical axis. Once the limits of the illuminated area are reached, concentrated around the optical axis, the NB underestimates the received optical power. This suggests that, while the NB provides a better local approximation compared to the Lambertian model, it still fails to offer a realistic representation of a VLC system using vehicle headlights as transmitters.

To enhance the representation of the low beam using a narrow beam based model, a slight downward tilt of the beam can be introduced. Additionally, the beam profile should be adapted in both the horizontal and vertical directions to better reflect the broader horizontal spread characteristic of actual low beams. A two-dimensional Gaussian beam model, employing different exponent values for the horizontal and vertical axes, offers a promising approach. This refinement is expected to yield significant improvements in model accuracy without introducing considerable complexity.

4 Conclusion

For realistic and regulation-compliant V-VLC performance evaluation, simplified Lambertian or narrow beam models fall short. The Lambertian model significantly overestimates received power in peripheral regions while underestimating it near the concentrated illumination zones of actual low beam (LB) headlights. This leads to an overestimation of system coverage and an underestimation of effective communication range.

The narrow beam model performs better, particularly near the LB cut-off region, but still overestimates received power along its optical axis and underestimates it elsewhere due to its limited spread. Moreover, achieving regulatory peak intensities with either model would demand substantially higher luminous flux, resulting in unacceptable glare.

In contrast, real world low beam headlights show a complex asymmetrical spatial profile, with sharp cut-off lines and steep intensity gradients. Accurately capturing this behaviour using simplified models is challenging. The most realistic representation is achieved via measured LIDs, provided these are applied at or beyond the limiting photometric distance, estimated around 17 m. At closer ranges, ray tracing simulations that account for the source's extended nature offer higher fidelity, though at the cost of computational complexity and increased variance due to their stochastic nature.

The optimal approach thus combines ray tracing for short-range scenarios with LID-based point source models at longer distances. Alternatively, a modified narrow beam model with a downward tilt and anisotropic beam spread, wider horizontally than vertically, could provide a practical and more accurate solution. Furthermore, daytime running lights, which operate continuously and exhibit simpler radiation patterns, merit investigation as viable V-VLC transmitters.

References

- AL-SALLAMI, F. M., BENKHELIFA, F., ASHOUR, D., GHASSEMLOOY, Z., HAAS, O. C. L., AHMAD, Z., and RAJBHANDARI, S. 2024. Average Channel Capacity Bounds of a Dynamic Vehicle-To-Vehicle Visible Light Communication System. *IEEE Transactions on Vehicular Technology*, 73(2), 1513–1523. <https://doi.org/10.1109/TVT.2023.3320889>
- ALSALAMI, F. M., AHMAD, Z., ZVANOVEC, S., HAIGH, P. A., HAAS, O. C. L., and RAJBHANDARI, S. 2021. Statistical channel modelling of dynamic vehicular visible light communication system. *Vehicular Communications*, 29, 100339. <https://doi.org/10.1016/j.vehcom.2021.100339>
- CAILEAN, A. M., and DIMIAN, M. 2017. Current Challenges for Visible Light Communications Usage in Vehicle Applications: A Survey. *IEEE Communications Surveys and Tutorials*, 19(4), 2681–2703. <https://doi.org/10.1109/COMST.2017.2706940>
- CIE 1996. CIE 121:1996. The Photometry and Goniophotometry of Luminaires. Vienna: CIE.
- DOTREPPE, G., AUDENAERT, J., SCHEIR, G., VAN DAN BOSSCHE, P. and JACOBS, V.A.J. 2023. Off-axis limiting photometric distance of Lambertians and narrow beams. *Lighting Research & Technology*, 56(6), 550-569. <https://doi.org/10.1177/14771535231208933>
- ERSO 2018. Motorways 2018. URL: <https://road-safety.transport.ec.europa.eu/system/files/2021-07/ersosynthesis2018-motorways.pdf> Last Accessed on: 09-04-2025
- GHASSEMLOOY, Z., POPOOLA, W. and RAJBHANDARI, S. 2019. Optical Wireless Communications: System and Channel Modelling with MATLAB. In *Optical Wireless Communications* (2nd ed.). CRC Press LLC. <https://doi.org/https://doi.org/10.1201/9781315151724>
- HASAN, M. K., ALI, M. O., RAHMAN, M. H., CHOWDHURY, M. Z and JANG, Y. M. 2022. Optical Camera Communication in Vehicular Applications: A Review. *IEEE Transactions on Intelligent Transportation Systems*, 23(7), 6260–6281. <https://doi.org/10.1109/TITS.2021.3086409>
- LIU, J., GUO, Z., SHAN, D., and LIU, X. 2023. Effective lane width for cars considering lateral oscillation characteristics based on high-precision field data. *International Journal of Transportation Science and Technology*, 16, 18–33. <https://doi.org/10.1016/j.ijst.2023.10.007>
- MEMEDI, A., and DRESSLER, F. 2020. Vehicular Visible Light Communications: A Survey. *IEEE Communications Surveys and Tutorials*, 23(1), 1–22. <https://doi.org/10.1109/COMST.2020.3034224>
- NDJIONGUE, A. R., and FERREIRA, H. C. (2018). An overview of outdoor visible light communications. *Transactions on Emerging Telecommunications Technologies*, 29(7), 1–15. <https://doi.org/10.1002/ett.3448>
- SHAABAN, R., and FARUQUE, S. 2020. Cyber security vulnerabilities for outdoor vehicular visible light communication in secure platoon network: Review, power distribution, and signal to noise ratio analysis. *Physical Communication*, 40, 101094. <https://doi.org/10.1016/j.phycom.2020.101094>
- SHAABAN, K., SHAMIM, M. H. M., and ABDUR-ROUF, K. 2021. Visible light communication for intelligent transportation systems: A review of the latest technologies. *Journal of Traffic and Transportation Engineering (English Edition)*, 8(4), 483–492. <https://doi.org/10.1016/j.jtte.2021.04.005>
- TEODOROVIĆ, D. and JANIĆ, M. (2017). *Transportation Engineering, 2nd Ed.* Oxford: Butterworth-Heinemann.
- TSENG, H.-Y., WEI, Y.-L., CHEN, A.-L., WU, H.-P., HSU, H., and TSAI, H.-M. 2015. Characterizing link asymmetry in vehicle-to-vehicle Visible Light Communications. *2015 In: Proceedings of the IEEE Vehicular Networking Conference (VNC), 16-18 December, 2015, Kyoto, Japan.* 88–95. <https://doi.org/10.1109/VNC.2015.7385552>
- UN/ECE 2009. Regulation No 87 — Uniform provisions concerning the approval of daytime running lamps for power-driven vehicles. ECE: Geneva
- UN/ECE 2013. Regulation No. 112 — Uniform provisions concerning the approval of motor vehicle headlamps emitting an asymmetrical passing beam or a driving beam or both and equipped with filament lamps and/or light-emitting diode (LED) modules. ECE: Geneva
- UN/ECE 2018. Regulation No. 48 — Uniform provisions concerning the approval of vehicles with regard to the installation of lighting and light-signalling devices [2019/57]. ECE: Geneva
- UN/ECE 2018. Regulation No 128 — Uniform provisions concerning the approval of light emitting diode (LED) light sources for use in approved lamp units on power-driven vehicles and their trailers [2018/1998]. ECE: Geneva
- UN/ECE 2021. Regulation No 149 – Uniform provisions concerning the approval of road illumination devices (lamps) and systems for power-driven vehicles [2021/1720]. ECE: Geneva
- VAN MIERLO, J., BERECIBAR, M., BAGHDADI, M. EL, DE CAUWER, C., MESSAGIE, M., COOSEMANS, T., JACOBS, V. A., and HEGAZY, O. (2021). Beyond the state of the art of electric vehicles: A fact-based paper of the current and prospective electric vehicle technologies. *World Electric Vehicle Journal*, 12(1), 1–26. <https://doi.org/10.3390/wevj12010020>
- WORLD HEALTH ORGANIZATION. 2018. *Global Status Report On Road Safety.* <https://www.who.int/publications/i/item/9789241565684> Last accessed on: 09-12-2024
- WORLD HEALTH ORGANIZATION. 2023. *Road traffic injuries.* <https://www.who.int/news-room/fact-sheets/detail/road-traffic-injuries> Last accessed on: 09-12-2024
- YAHIA, S., MERAIHI, Y., RAMDANE-CHERIF, A. and BENMESSAOUD, A. 2021. A Survey of Channel Modeling Techniques for Visible Light Communications. *Journal of Network and Computer Applications*, 194(December 2020). <https://doi.org/10.1016/j.jnca.2021.103206>